Cinder Cone Growth Modeled After Northeast Crater, Mount Etna, Sicily

THOMAS R. MCGETCHIN,[1] MARK SETTLE, AND BERNARD A. CHOUET

Department of Earth and Planetary Sciences, Massachusetts Institute of Technology Cambridge, Massachusetts 02139

Northeast crater is a pyroclastic cone near the summit of Mount Etna, built to its present volume (1×10^6 m^3) by nearly constant strombolian activity since its birth in 1911. Detailed analysis of one typical photograph of a June 1969 eruption indicates that particles exit with a median velocity of about 51 m/s at angles distributed nearly uniformly between 70° and vertical. Ejecta consists of ash to 1-m bombs. Physical properties of ejecta include median bomb density, 1.53 g/cm^3; particle size of ash found locally on the cone, 150 μ; median size of bombs constituting the cone, 15 cm; sphericity of bombs, 0.78; and surface roughness of bombs, approximately 0.05. Ballistic analysis using these data and including effects of atmospheric drag shows that cinder cone morphology can be predicted by a quantitative model that is in excellent agreement with observed cone features. Cone shape or profile, rim location, limit of continuous ejecta, the ballistic limit (maximum range of ejected fragments), and the size and location of talus slopes are uniquely determined by fragment exit conditions and ballistics. The model suggests that cinder cones grow through four distinct stages: (1) simple cone, with mantle bedding and a low rounded rim, (2) onset of an exterior talus slope, (3) destruction of the original rounded rim by backward migration of the talus, and (4) outward growth of the talus slope beyond the ballistic limit. In the lunar exterior ballistic environment, cinder cones (if they erupted at conditions qualitatively similar to Etna's Northeast crater) should form tuff rings with low, barely discernible rims. Small dark halo craters and dark mantling deposits observed on the moon (such as those near the Apollo 17 site) may be lunar equivalents of normal terrestrial cinder cones. Clusters of such lunar cones might form continuous blankets rather than groups of discrete cones as they do on the earth. Martian cones, formed under the same conditions, would be more like lunar cones than terrestrial ones.

This paper presents results of a study of the mode of growth of cinder cones. It focuses on structure, physical properties of ejecta, ballistics, and growth of Northeast crater, a young pyroclastic cone that originated in 1911 near the summit of Mount Etna, Sicily. We describe the cone and the physical properties of the ejecta and relate these properties to the ballistics of the ejecta revealed by an analysis of a photograph taken of Northeast crater in a typical state of eruption in June 1969. From the eruption photography we obtain statistics on ejection velocity and ejection angle for the ejected particles. We use these data to discuss two problems: (1) the mode of growth of Northeast crater and of cinder cones in general and (2) the structure and surface morphology of cinder cones such as Northeast crater on the surface of Mars and the moon, if they were formed under similar eruption conditions. Both problems are approached by exploring the distribution of ejecta and the growth of cones by repeated similar eruptions, the effect of atmospheric drag and gravity on the trajectories of particles being taken into account.

Published work on Etna is largely in the European literature and has been summarized by *Rittmann* [1963], *Tazieff* [1960], *Imbo* [1965], and recently by *Pichler* [1970]. Recent work includes a field excursion guide by *Tazieff* [1971], a description of the 1971 eruption [H. Tazieff and F. LeGuern, unpublished field studies, 1971; *Rittmann*, 1971; *Tanguy*, 1971], a brief description of the lavas and the possible tectonic control of their evolution [*Rittmann*, 1963; *Romano*, 1970], a description of Valle del Bove and its structure, lavas, and evolution [*Klerkx*, 1968, 1971; *Kieffer*, 1970], discussions of the petrology [*Tanguy*, 1966, 1967, 1968, 1971] and viscosity [*Walker*, 1967] of the Etna lavas, and a description of the emplacement of the submarine lavas [*Moore et al.*, 1970].

Published work on cinder cones and related topics includes descriptive accounts by *Lyell* [1850], *Becker* [1885], *Cotton* [1944], *Jagger* [1947], *Bullard* [1962], and *Porter* [1972]. More recently, books by *Macdonald* [1972] and *Green and Short* [1971] contain photographs illustrating the development of pyroclastic cones (in particular, note Green and Short's Figures 48–58, which can be compared with our Figure 14). Several recent papers have appeared describing specific structural or physical aspects of pyroclastic deposits [*Fisher*, 1964; *Fisher and Waters*, 1970, 1971; *Waters and Fisher*, 1971; *Heiken*, 1971, 1972; *Sheridan*, 1971]. Other authors have discussed the mechanics of airborne ash falls (far-field deposition), notably *Lamb* [1970], *Eaton* [1964], *Knox and Short* [1964], and *Wilcox* [1959], all of whom based their discussions at least in part on careful studies of tephra from Hekla, Iceland, by *Thorarinsson* [1951, 1967]. *Foshog and Gonzalez* [1956] reported quantitatively on the growth of Parícutin. *Scott and Trask* [1971] recently published a detailed description of 17 Quaternary cones in Nevada, and *Porter* [1972] has described the cinder cones of Mauna Kea, Hawaii. Chouet has recently completed a very detailed study of eruption movies of Stromboli that reveal much quantitative information about the kind of activity responsible for cinder cone growth [*Chouet*, 1973; *Chouet et al.*, 1974].

REGIONAL SETTING

Mount Etna and Sicily lie on a line of apparently related tectonic features stretching from the Apennine Mountains of the Italian peninsula to the Atlas Mountains of northern Africa. Sicily and the lower section of Italy are collectively referred to as the Calabrian arc. The volcanic features included are the active volcanoes of the Roman province (in-

[1] Now at Division of Mineral Sciences, Smithsonian Institution, Washington, D. C. 20560.

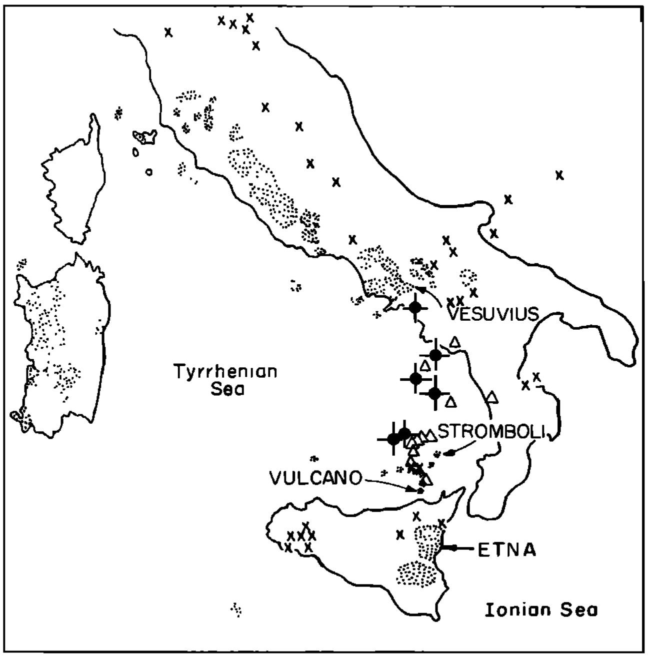

Fig. 1. Map showing the location of Etna and the other Tertiary volcanic provinces (shaded areas) of the western Mediterranean and seismicity [*Erickson*, 1970]. Crosses indicate earthquake focal depths of 0–70 km; triangles, 71–300 km; spiked circles, 301–700 km.

cluding Vesuvius and Ischia), the Aeolian Islands north of Sicily (Vulcano and Stromboli), and the islands southwest of Sicily (including Pantellaria). Critical to understanding the tectonic setting, hence the local geology, the volcanism, and the local history, is the relationship between the Calabrian arc and the Ionian and Tyrrhenian basins, which flank the tectonic trend line straddled by Mount Etna (Figure 1).

The Italian peninsula has experienced shallow seismicity (less than 50 km) throughout historical time, although recent activity appears to be preferentially distributed in the Apennine Mountains and eastern Italian coastal areas [*Erikson*, 1970]. Intermediate-depth ($100 > d > 50$ km) earthquakes are present in the region and are concentrated, with deep quakes (>100 km), in a north-striking band in the southeast corner of the Tyrrhenian, between Sicily and Naples. From a study of the fault plane solutions of deep-focus earthquakes *McKenzie* [1970] concluded that a slab dipping to the west underlies the southeast Tyrrhenian Sea. *Ryan et al.* [1971] found low sediment thicknesses and thin sedimentary aprons in the Tyrrhenian. They also observed a correlation between several magnetic anomaly trends and topographic troughs in the Tyrrhenian sea floor. Gravity data [*de Bruyn*, 1955] show that the Tyrrhenian basin is not isostatically balanced but has local positive anomalies (250 mg) indicating a mass excess. These observations, together with the observed high heat flow [*Fahlquist*, 1963] and abundant volcanic seamounts and islands, led Ryan et al. to conclude that the Tyrrhenian is a young extensional feature. By contrast, the Ionian Sea is seismically quiet, is deeper, contains a greater thickness of accumulated sediment, and has a heat flow equal to or less than the world average. The floor of the Ionian contains no apparent systematic distribution of magnetic anomalies and appears to be tectonically stable.

Historical volcanic activity is associated with the lower third of the Italian peninsula (Vesuvius and Ischia), Sicily (Etna), and the Aeolian Islands (Stromboli and Vulcano). *Gasparini and Adams'* [1969] K-Ar dating defines a recent episode of volcanic activity throughout the southern third of the Italian peninsula. There is no reported occurrence of volcanism within the Ionian Sea.

The current generally accepted interpretation of the regional tectonics is that Sicily represents a crustal splinter that was translated to its present position as Italy rotated counterclockwise from its previous position juxtaposed against the southeastern coasts of Spain and France. Independent geological evidence from Corsica [*Stanley and Mutti*, 1968], the Red Sea, and the Gulf of Aden [*Girdler*, 1968] implies clockwise rotation of the African continent in Tertiary time relative to the Eurasian and Arabian plates. Three major tectonic events are recognized by *Ryan et al.* [1971] and *McKenzie* [1970], which may or may not overlap in time or cause. The first event is the construction of the folded mountain chain (Apennine to Atlas ranges) that crosses Sicily in a WSW-ENE direction and underlies Etna. The second is the counterclockwise rotation of the Italian peninsula relative to the Eurasian plate. The third and apparently currently active event is the northward underthrusting of the African plate beneath Eurasia. Some left lateral gliding of the African plate

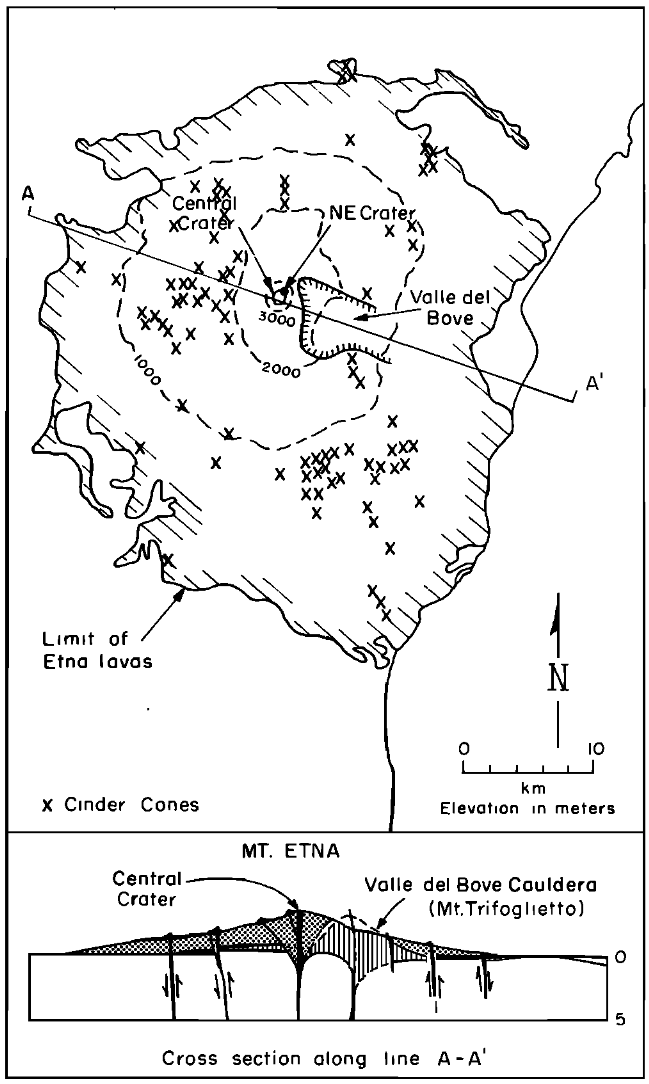

Fig. 2. Map of Mount Etna and the vicinity and a generalized geological cross section along a line east-west through the Etna summit [*Rittmann*, 1965]. Cinder cones are represented by crosses.

past the European plate in the vicinity of Sicily is possible and perhaps, in fact, produces the counterclockwise motion of present-day Italy.

The geology of Etna and the genesis and evolution of its lavas are problems of quite general interest for two reasons: (1) the unusual tectonic situation, apparently involving active subduction of a continental plate (Africa) under another continental plate (or at least a fragment of one, Sicily), and (2) the apparent persistence of Etna as a point source of magma for a long period of geologic time over an active tectonic zone.

Etna

Mount Etna is a large, symmetrical, low cone built of basalt and andesite on the east coast of Sicily. Its base is about 60 × 40 km, and it is presently about 3300 m high. The lower 2900 m is a shield built of basaltic lavas; the upper 400 m is mixed pyroclastics and flows (composite cone or stratovolcano). Slopes near the summit average about 25° and gradually decrease on all sides to 2° or 3° at the sea. Catania, the city that lies about 30 km to the south, has been threatened by several historic eruptions and was partially buried by flows and ash in 1169 and 1669 (Figure 2). The summit crater at Etna, called Central crater, contains a nearly circular vent 350 m in diameter with almost vertical walls. The rocks exposed in the walls are interbedded fine-grained pyroclastics and lava. The depth of the central vent is unknown but exceeds a measured 850 m (H. Tazieff and F. LeGuern, unpublished field studies, 1971). Northeast crater is a composite cone built on the shoulder of Central crater about 600 m northeast from the summit.

Rittmann [1963] reviewed the local geological setting of Etna. The edifice of the volcano is Pleistocene in age, but the activity began as early as Triassic with effusive submarine lavas. Activity continued through the Jurassic, Cretaceous, and Tertiary. Etna itself consists of several overlapping cones built on structural horsts. With time the activity has migrated westward. The volcano is built in an ancient gulf on the east coast of Sicily, surrounded by mountains made of Eocene and Miocene sedimentary rocks. Etna now dwarfs these older structures.

The Etna lavas are generally andesites but range in SiO_2 content from 47 to 57%. *Romano* [1970] recognized several distinct differentiation trends that begin with olivine basalt and evolve to hawaiites (alkali-latite and alkali-andesite), to latite-andesite, or to phonolitic nepheline tephrite. The lavas

TABLE 1. Chemical Compositions, Weight Percent Norms, and Reported Modes for Etna Lavas

	ET 8 (1)	ET 12 (2)	ET 13 (3)	ET 14 (4)	ET 25 (5)	ET 26 (6)	ET 27 (7)	ET 28 (8)	ET 29 (9)	ET 30 (10)	ET 31 (11)	ET 32 (12)
Element												
SiO_2	48.46	47.34	46.69	46.67	48.80	50.00	51.60	47.38	47.53	47.01	47.22	47.14
Al_2	15.92	17.52	16.76	16.45	18.50	18.70	18.80	17.09	17.44	17.21	17.23	16.94
Fe_2O_3	3.42	5.37	6.10	6.15				3.15	6.00	6.83	5.25	5.41
FeO	8.00	5.76	6.36	6.31	9.70	9.00	8.20	7.59	5.16	4.44	5.80	5.68
MgO	5.05	5.34	5.24	4.58	4.10	3.50	2.70	5.50	5.52	5.54	5.61	5.58
CaO	10.90	10.51	10.57	11.54	10.40	9.20	7.90	10.32	10.77	10.77	10.73	10.74
Na_2O	4.13	4.06	4.66	4.45	4.8	5.60	6.40	4.00	3.42	3.40	3.42	3.64
K_2O	1.61	1.37	1.51	1.76	2.00	2.40	3.20	1.75	1.71	1.72	1.69	1.68
H_2O^+	0.01	0.12	0.03	0.05					0.50	0.11	0.42	0.20
H_2O^-	0.03							0.06	0.06	0.18	0.15	0.09
TiO_2	2.03	1.80	1.82	1.75	1.70	1.50	1.20	1.68	1.68	1.66	1.69	1.71
P_2O_5	0.65	0.35	0.39	0.31				0.38				
MnO	0.12	0.18	0.15	0.13				0.18				
BaO			0.16									
Total	99.81	99.72	100.44	100.15	100.00	100.00	100.00	99.08	99.79	98.87	99.21	98.81
CIPW norms												
Q	0.0	0.0	0.0	0.0	0.0	0.0	0.0	0.0	0.0	0.0	0.0	0.0
OR	9.53	8.12	8.88	10.39	11.82	14.18	18.91	10.44	10.13	10.28	10.07	10.05
AB	25.37	23.07	18.74	15.24	13.46	15.92	17.16	18.68	20.99	21.02	19.83	19.50
AN	20.67	25.61	20.27	19.68	23.03	18.80	13.12	23.73	27.24	26.92	26.88	25.22
NE	4.73	6.17	11.12	12.11	14.71	17.05	20.07	8.39	4.34	4.38	5.06	6.33
WO	10.60	10.18	12.40	14.81	11.93	11.21	10.89	10.62	10.98	11.32	11.18	11.98
EN	5.97	7.33	8.73	10.18	4.87	4.32	3.80	6.15	8.66	9.79	8.11	8.84
FS	4.20	1.93	2.62	3.44	7.15	7.05	7.38	3.99	1.10	0.00	2.04	2.00
FO	4.65	4.21	3.00	0.85	3.75	3.08	2.05	5.38	3.59	2.92	4.19	3.66
FA	3.60	1.22	0.99	0.32	6.07	5.55	4.40	3.85	0.50	0.00	1.16	0.91
IL	3.86	3.43	3.44	3.32	3.23	2.85	2.28	3.22	3.20	3.19	3.24	3.29
AP	1.54	0.83	0.92	0.73	0.0	0.0	0.0	0.91	0.0	0.0	0.0	0.0
MT	4.97	7.81	8.81	8.90	0.0	0.0	0.0	3.61	8.72	9.61	7.67	7.94
Reported modes												
Plagioclase								29.80	17.10	18.50	17.50	19.40
Augite								11.20	13.00	9.20	10.80	8.40
Olivine								3.30	2.70	4.70	2.50	2.60
Ti-magnetite								2.80	1.70	1.00	1.30	1.20
Groundmass								52.90	65.50	66.60	67.90	68.30

All values are in weight percent.

Number in parentheses beneath sample number is the analysis number.

ET 8, andesine basalt, lava of 1910, analyzed by Washington [*Imbo*, 1965]; ET 12, basalt, lava of 1928 (Bocche delta Nuca), analyzed by Strabba [*Imbo*, 1965]; ET 13, augitic basalt, lava of 1950 to 1951, analyzed by Cumin [*Imbo*, 1965]; ET 14, augite olivine basalt, lava of 1956, analyzed by Silvestri [*Imbo*, 1965]; ET 25, lava, Northeast crater, analyzed by *Tanguy* [1968]; ET 27, lava, lateral eruption of Mount Etna, analyzed by *Tanguy* [1968]; ET 28, subterminal lava, September 23, 1967, northern slope of Northeast crater, analyzed by la Source [*Tanguy*, 1971]; ET 29, lava flow from the south vent, May 7, 1971, analyzed by Lenoble [*Tanguy*, 1971]; ET 30, lava flow from the upper east vent, May 7, 1971, analyzed by Lenoble [*Tanguy*, 1971]; ET 31, lava flow from vent in Valle del Bove, May 9, 1971, analyzed by Lenoble [*Tanguy*, 1971]; ET 32, lava flow from lower Citelli vent, May 12, 1971, analyzed by Lenoble [*Tanguy*, 1971].

are alkaline, characterized by unusually high soda, but they are transitional to calc-alkaline types and have not evolved uniformly in time in any systematic way. Rather, an alkali-olivine basalt rich in normative nepheline recurs with time (Table 1). The Etna lavas are apparently fed to the surface from an upper mantle source, a view suggested by a very low $^{87}Sr/^{86}Sr$ ratio in spite of the high alkali content of the lavas.

Romano [1970] feels that the chemical variation of the Etna lavas can be accounted for by evolution from an olivine basalt parent magma (47% SiO_2) by the following: (1) gravitational settling of olivine and augite or olivine, augite, and calcic-anorthite in a low P_{H_2O} environment producing hawaiites and mugearites (alkali-andesites and latites); (2) separation of olivine and augite, gas transfer enriching the melt in Na, Ti, and Fe^{3+}, producing tephritic phonolite; and (3) gravitational settling of olivine, augite, and hornblende in a high P_{H_2O} environment producing a calc-alkaline trend culminating in latite-andesite (Figure 3). Lavas currently being produced at Northeast crater show a tendency to become progressively more tephritic (and rich in normative nepheline) with time, perhaps owing to Na enrichment resulting from continuous fumarolic activity [*Tanguy*, 1966].

The activity of Etna in historic times is highlighted by the violent eruptions of 1169, 1669, and 1766. Eruptions of three types are observed: (1) summit eruptions in a central crater, which produce flows and gas; (2) lateral eruptions along fissures radial from the central crater, which produce lava and minor amounts of pyroclastics (5–8%); and (3) so-called eccentric eruptions, which produce scattered individual cones and flows (10% pyroclastics). The eruption of 1971 was of the second type, flows occurring along three separate radial fissures. Northeast crater is located on such a radial fissure (Figure 4).

The production rate of lava from Etna has averaged about 8×10^6 m^3/yr since 1669 and 5×10^6 m^3/yr in the last 70 years. The latter rate would produce a layer about 5 m thick every 1000 years if it were spread uniformly over the surface now occupied by the Etna lavas or would raise the summit about 15 m/yr in altitude if it were added conically to the mountain. The lava production at Etna is considerably less than that at Kilauea, Hawaii, which was estimated to be 30×10^6 m^3/yr by *Stearns and MacDonald* [1946] but ranges up to 180×10^6 m^3/yr during more vigorous periods [*Swanson*, 1971]. The total volume of Northeast crater is about 1×10^6 m^3, or about 20% of the average annual output of Etna; hence it is a volumetrically trivial feature relative to Etna itself.

During the April–May 1971 Etna eruption Northeast crater became completely inactive. It stopped its normal activity several days before the rift eruption started on April 5 and was inactive until our departure on September 1, 1971. It appears that this eruption tapped the source normally feeding Northeast crater and that the lavas were temporarily diverted into the radial fissures. Analyses 9–12 (Table 1) are from the 1971 eruption [*Tanguy*, 1971] and are generally similar to analyses 5 and 8 (Northeast crater lavas), although the new lavas are depleted in normative nepheline and total iron relative to previously analyzed Northeast crater rocks.

NORTHEAST CRATER

Northeast crater (Bocca Nord-Est) lies about 300 m northeast of the main central summit vent (Central crater) about 600 m from the summit of Etna (Figures 5 and 6). It originated during the eruption of 1911 and has been in an almost continuous state of activity since, pausing only when activity breaks out elsewhere on the mountain [*Tazieff*, 1971], as in 1971. The cone measures about 230 × 200 m across its base

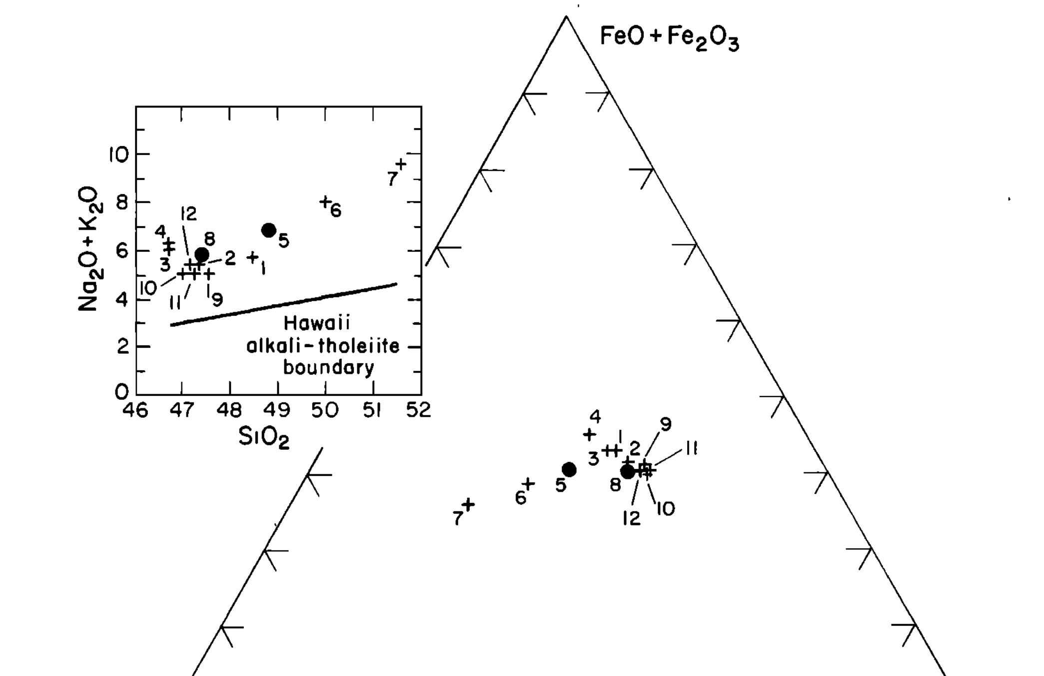

Fig. 3. Variation diagrams for Etna lavas. The large triangle is an AMF diagram including rocks from the 1971 eruption and Northeast crater. The small insert is a $Na_2O + K_2O$ versus SiO_2 diagram for the Etna lavas. Plus signs represent Etna lavas; solid circles, Northeast crater. Numbers refer to analyses in Table 1.

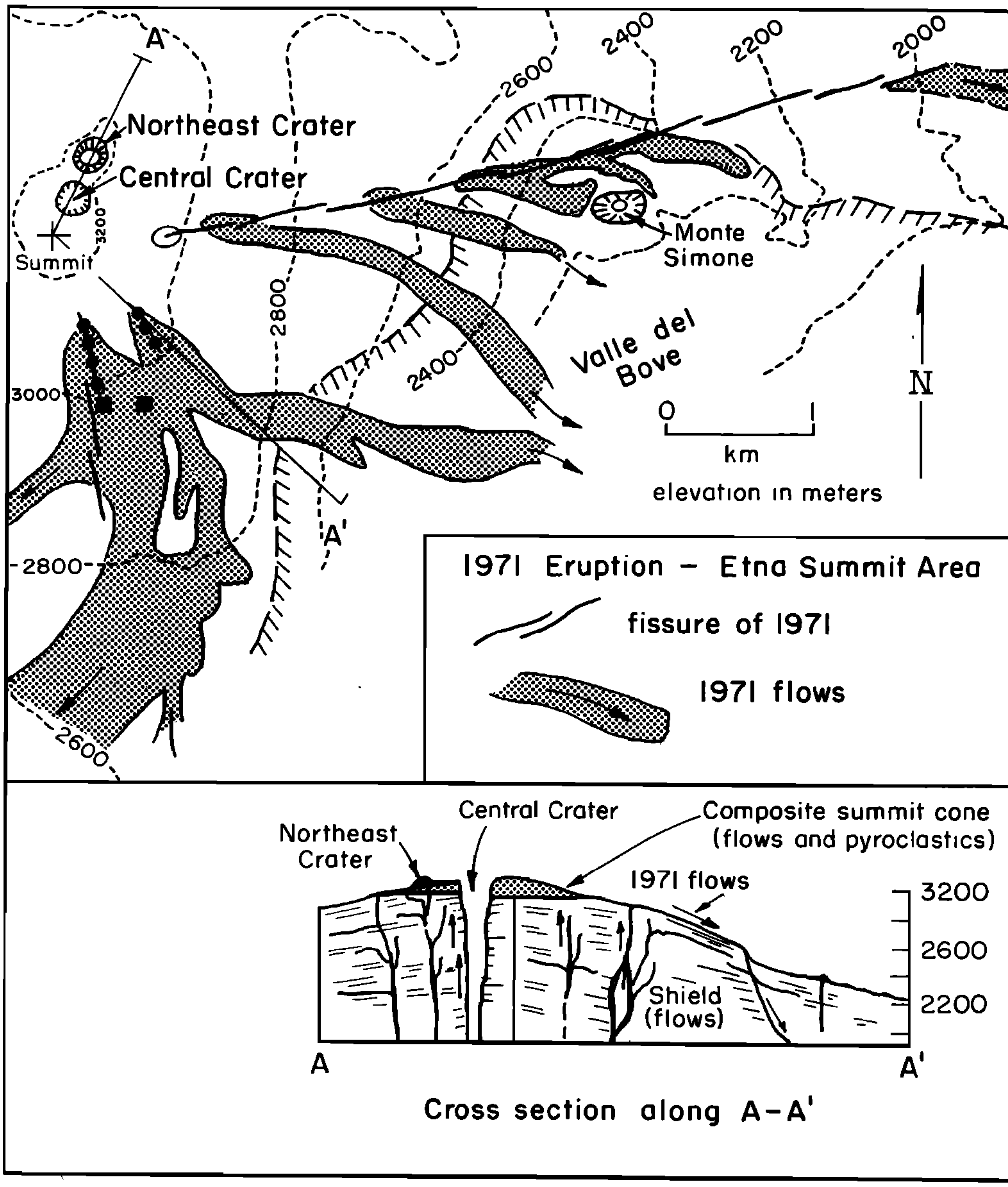

Fig. 4. Sketch map and cross section of the summit of Etna showing the location of Northeast crater and the flows associated with the 1971 eruption.

and varies in height with time owing to both collapse and removal of the summit during especially violent eruptions. In September 1971 its summit was about 30 m above the surrounding terrain; slightly over a year earlier in June 1970 it was nearly 60 m high. Outer slopes average between about 31° and 38°, the apparent angle of repose; inner slopes vary from nearly vertical at the rim to inward-dipping talus piles sloping about 30° farther down inside the crater. In August 1971 the crater floor was a broad inverted cone produced by the intersection of talus from the inner walls. A year earlier two active vents cut a flat-floored summit pit. In the mid-1960's a small lava lake was reported in the floor of Northeast crater (A. Nicoloso, personal communication, 1971). A strong prevailing wind blows from the northwest, commonly at velocities estimated at 100 km/hr (Figure 7).

Typical activity consists of effusion of small flows from just north of the cone, together with small central eruptions. The strength of the central eruptions at Northeast crater occasionally reaches paroxysmal proportions that blow the summit of the crater away. The summit also is routinely reduced by collapse into the vent, but it systematically builds itself up again, so that the shape of the cone is constantly changing. Ejection of pyroclastics and emission of gases have been observed concurrently in different vents, and small lava ponds have formed within the crater, according to local guides.

Typical central eruptions have durations of several seconds, and repose periods vary from several minutes to several days. Time exposure photographs of eruptions at night clearly reveal the following. (1) Trajectories are commonly strongly shifted to the southeast by the wind. (2) Large particles (estimated from the track width) exit at low velocities and only barely clear the rim. Upon impact just beyond the rim the largest fragments roll down the slope. (3) Small fragments are ejected at higher velocities. (4) The two jets active in June 1970 show clearly in the photographs.

The surface of the cone is covered with ejecta, mainly scoria, that varies from ash with a median grain size of about

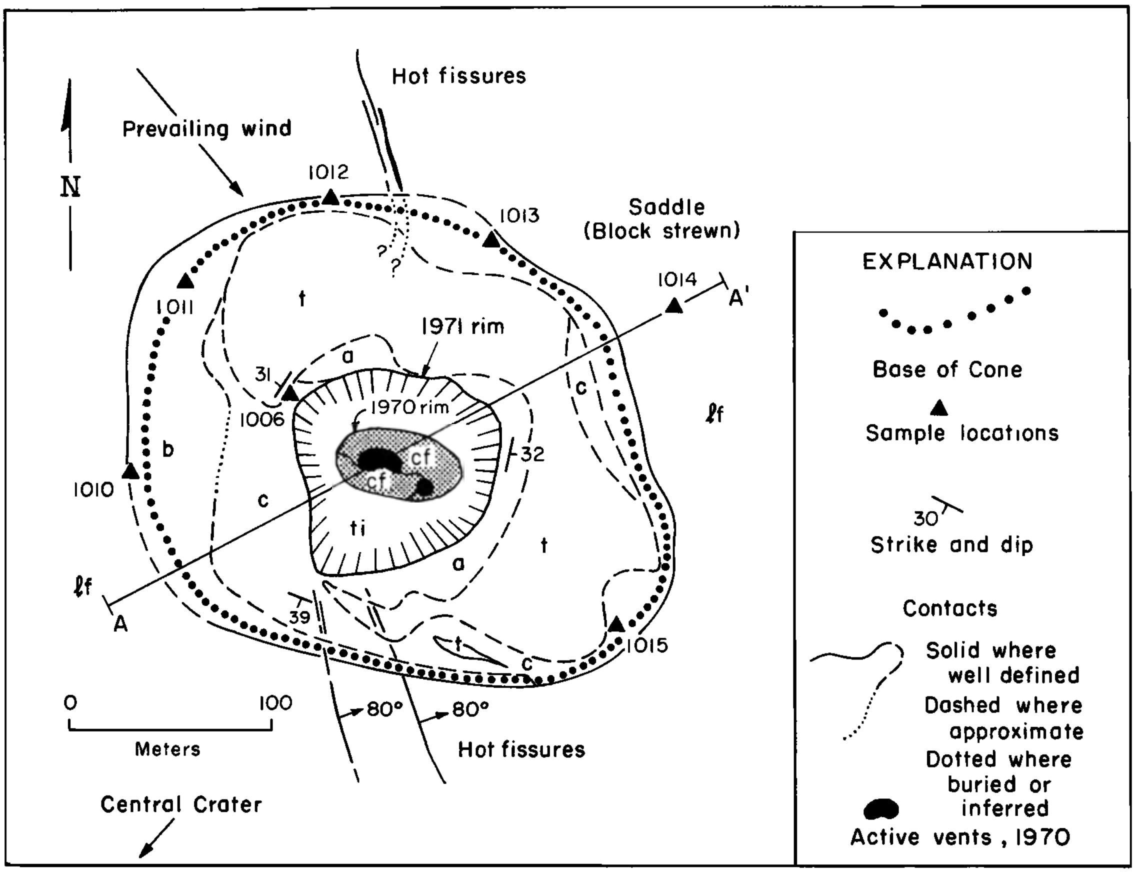

Fig. 5. Geologic sketch map of Northeast crater. The locations of the rim in September 1971 and June 1970 are shown. Triangles show stations where a fragment population count was made. The cross section (A-A′) is shown in Figure 7. Map units are: *b*, annular ring of boulder-sized fragments at the base of the cone consisting of large bombs (30–100 cm) that have rolled down the cone to their present position; *c*, surface covered by fragments averaging 10–30 cm; *a*, ash, most in the millimeter range with occasional large blocks present, concentrated near the rim; *t*, talus exterior to crater rim, dipping outward at 30° or more and consisting of mixed ash and blocks (predominantly ash), thinly bedded, parallel to the slope; *ti*, talus slopes on the interior of the crater, composed of material derived from inner crater wall (mainly ash mixed with bombs); dark areas in the center of the crater are vents observed in action in June 1969; and *cf*, flat crater floor observed during June 1969. A fissure system crosses the cone in a NNW-SSE direction.

Fig. 6. Photograph of Northeast crater taken from the southwest. This photograph was taken from near the rim of Central crater looking northeastward toward Northeast crater. Many of the features described in the geologic map are visible, including the annulus of boulders at the base of the cone, the exterior and internal talus, and the ash-rich unit near the rim. The fissure system with hot fumaroles is clearly visible. Notice the people near the center of the photograph. The sample of 94 bombs described later was taken from near the center of the slope of the cone, left of the center of the photograph and just left of the foot path, which is barely visible in the photograph.

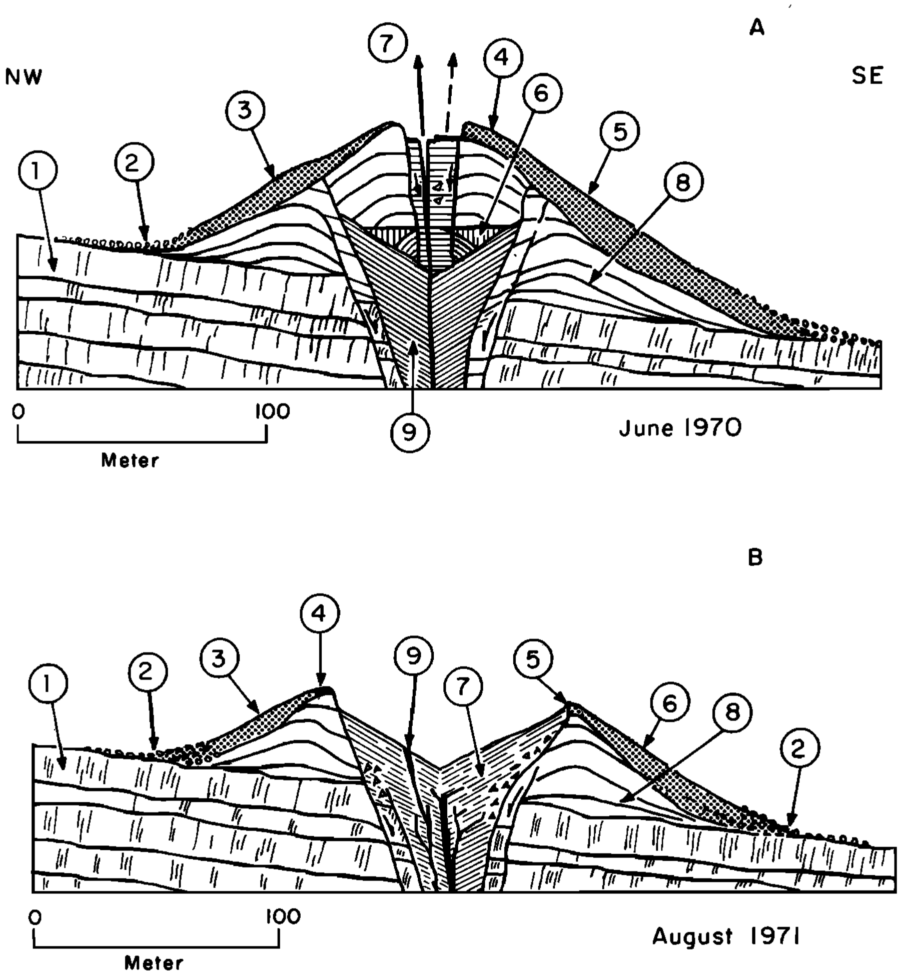

Fig. 7. Geological cross sections of Northeast crater. The line of section is A-A′ (Figure 5) and runs from northwest to southeast through the center of Northeast crater. (*a*) June 1970. Northeast crater is built on a surface of flows and pyroclastics from the summit crater of Etna (1). Surrounding the base of the cone is an annular ring of boulder-sized fragments, commonly up to 1 m in diameter (2). The surface of the cone is covered with talus consisting of 10- to 30-cm fragments (3) and ash locally (4) and talus consisting of mixed ash and bombs (5). Small transient lava ponds observed in the bottom of the crater (6) have been subsequently buried by later ejecta or destroyed by collapse or large eruptions. Two jets were active during June 1969, one ejecting incandescent bombs and scoria and the other ejecting mainly gas (7). The floor of the crater at that time was a flat surface probably consisting of nearly horizontally bedded fallback. The cone is inferred to be built upon a simple cinder cone (stage 1 type, explained in text) consisting of ejecta with similar bedding and a low rounded rim located about 60 m from the vent (8). The vent (9) is assumed to be clogged with inherited inward-dipping talus. (*b*) August 1971. The general features of the crater are similar, but outward-dipping bedded talus ash is exposed in vent walls (5), the interior of the crater is filled with inward-dipping talus derived from the vent walls (7), and the active vent that fed the surface prior to the spring 1971 eruption is now dormant (9) and covered thinly with talus.

150 μ to blocks up to 1 m in diameter. The ash is concentrated on the downwind sides of the cone (toward the southeast). The outer slopes of the crater consist of talus, mostly ash on the northeast and south sides of the crater, and cobbles averaging 10 cm on the northwest and west sides. The wind clearly has controlled the distribution of ejecta, winnowing away fine material from ejecta deposited on the southeast side, and an unknown proportion of fine ash is carried far downwind to the southeast.

A circumferential ring averaging about 30 m in width and consisting of coarse blocks ranging from 30 cm to 1 m in diameter circles the crater at the base of its outside slopes. Large bombs lobbed over the rim roll to the base of the slope, whereas small (10 cm) blocks are decelerated by the roughness of the slope and remain behind to build up the surface at the angle of repose. Some coarse fragments land and remain on the rim, so that large blocks are found both on the rim and in the annulus surrounding the base of the cone.

Ejecta fragments of several types were observed: (1) dull gray to black moderately vesicular bombs (60–90%), (2) black highly vesicular cinders, commonly having an irridescent sheen (0–20%), (3) dense dark gray bombs (3–30%), and (4) brick red to orangish gray vesicular bombs (0–30%).

The true size distribution of material ejected by any given eruption is a mix of coarse bombs, found concentrated on the upwind surfaces of the crater, and ash preferentially distributed downwind; hence the size frequency distribution of the bulk ejecta is unknown. Two analyzed samples of ash have median particle sizes of 150 μ and 1.5 mm (Figure 8). Particle counts were made at seven sites, from which size frequency distributions were constructed. The largest bombs are just over 1 m in diameter; the median size varies from 10 to 30 cm. The contribution of fine particles generally is very minor, and the material is well sorted, 50% of the material falling between about 10 and 40 cm (Figure 8).

Ninety-four bombs in the 10- to 30-cm size range were

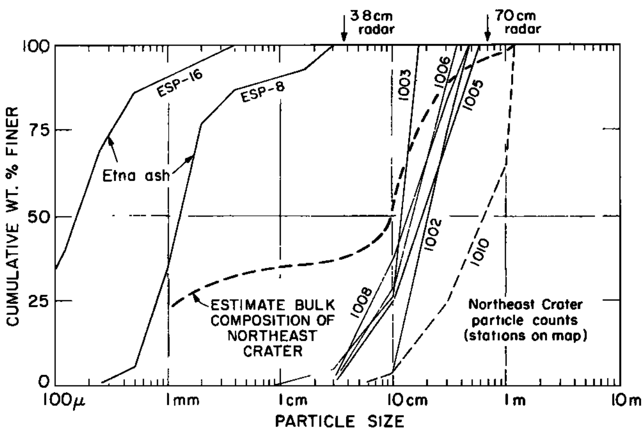

Fig. 8. Particle size frequency distributions of Northeast crater and Etna ejecta. Northeast crater samples generally have median sizes between 10 and 30 cm. Ash samples from 1971 vents have median sizes between 100 μ and 1 mm. The estimated bulk composition of Northeast crater as presently constituted is shown by the heavy dashed line. Probably typical Northeast crater ejecta, however, has a significantly larger component of fine-grained material (ash) that is systematically removed by wind and only partially retained near the cone. It is estimated that the median size of such bulk ejecta may be about 1 cm. Arrows indicate wavelengths of the most commonly used radar wavelengths (3.8 and 70 cm).

collected from the west side of Northeast crater near station 1003 and returned to the laboratory, where bulk densities were measured. Because the fragments were vesicular and somewhat permeable, emersion techniques, using Archimedes' principle, required modification (Figure 9). Each fragment was emersed in paraffin to seal off the surface after initial weighing. It was then immersed in water, and after a correction for the weight and volume of the paraffin was made, the bulk density of the fragment was calculated (Figure 10). Measured densities range from 1.2 to 2.8 g/cm^3, and the median density was 1.53 g/cm^3. Fifty percent of the fragments have densities between 1.35 and 1.92 g/cm^3; 90% have densities between 1.25 and 2.15 g/cm^3.

Particle shape and surface roughness are important from the viewpoint of exterior ballistics because they affect the drag experienced during flight. Measured sphericity (as defined by area) varied between 0.41 and 0.98; median sphericity was 0.78. Surface roughness is commonly expressed as the dimensionless quantity relative roughness ϵ/D, where ϵ is the magnitude of the surface irregularity and D is some characteristic linear dimension of the particle such as diameter. The surface of a typical 10-cm bomb consists of broken vesicules and is qualitatively rough. The largest vesicules are of the order of 1 cm deep; more typical ones are 3–5 mm deep. Relative roughness of Northeast crater ejecta probably ranges from about 0.02 to 0.10, the average being about 0.05. The drag law assumed for volcanic ejecta should include these factors.

The internal structure of Northeast crater can be observed in part and inferred in some detail from the cross sections shown in Figure 7. The interior walls observed in the summit crater consist of nearly horizontal to outward-dipping layered pyroclastics (ash and bombs). Some bomb-rich layers are well cemented, and rare flows may have spilled over the summit. The vent itself is filled with talus from the collapse of the vent walls, directly deposited pyroclastics, and lava intruded from below. The present exterior surface of the cone is built of superimposed talus, deposited layer upon layer by collapse of the oversteepened slope above. We infer that a layer of boulder-sized bombs underlies the outer part of the cone at the interface with the older flows.

Eruption Conditions at Northeast Crater and Ballistic Distribution of Cinder Cone Ejecta

Particle trajectories can be used to determine the conditions of ejection (that is, initial velocity and ejection angle). The coordinates of the apex of a trajectory in a vacuum uniquely and simply define the entire trajectory, including launch angle and velocity. The trajectories of volcanic ejecta such as those in Figure 11 clearly are not parabolas owing not only to cross wind and atmospheric drag but also to viewing angle and azimuth of the trajectory. Furthermore, volcanic ejecta is transported in and launched from a transient gas-rich jet. Upon encountering the atmosphere, these particles undergo deceleration according to their size, shape, density, and velocity. The jet influences the trajectories of the particles to some distance above the vent until it decays by viscous interaction with the atmosphere. Clearly, stereopsis is required to resolve the trajectories in three-dimensional space. Viewed (or photographed) from different sides, a volcanic jet presents many trajectories, only a few of which are parallel to the film plane. Without stereopsis, an angular ambiguity always exists; this ambiguity, however, can be treated statistically if radial symmetry can be assumed and if the location of the camera station is known precisely, so that the geometric relationship between the camera and the jet axis is known. These problems have been discussed in detail by *Chouet* [1973] and *Chouet et al.* [1974].

We analyzed one eruption of Northeast crater by using a photograph taken in June 1969. This eruption was typical of many similar ones photographed. The apexes of 289 trajectories were located in the image and corrected for the angle between the jet and the camera angle. Next we assumed that particles averaged about 10 cm in size (perhaps an overestimate) and calculated the effect of atmospheric drag as if they were ejected from the vent into a still atmosphere (that is, ignoring the effect of the jet itself). The exit conditions were inferred from the coordinates of the apex of each particle trajectory, and a statistical correction was applied for their

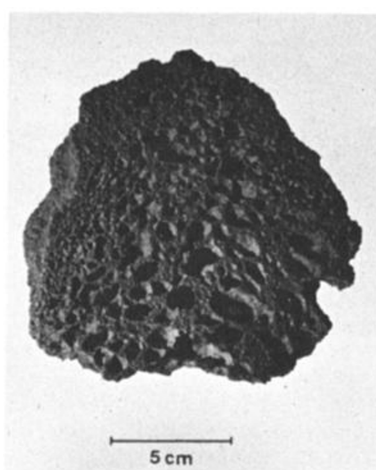

Fig. 9. Photograph of a cross sectional slice through a typical Northeast crater bomb. A rind consisting of fine vesicules (<5 mm in diameter) can be seen around three sides of the bomb, whereas the core and lower surface of the bomb consist of larger (>1 cm) vesicules. The vesicules are deformed. These features suggest that the outer surface is a quenched rind and that the bomb was deforming during its flight.

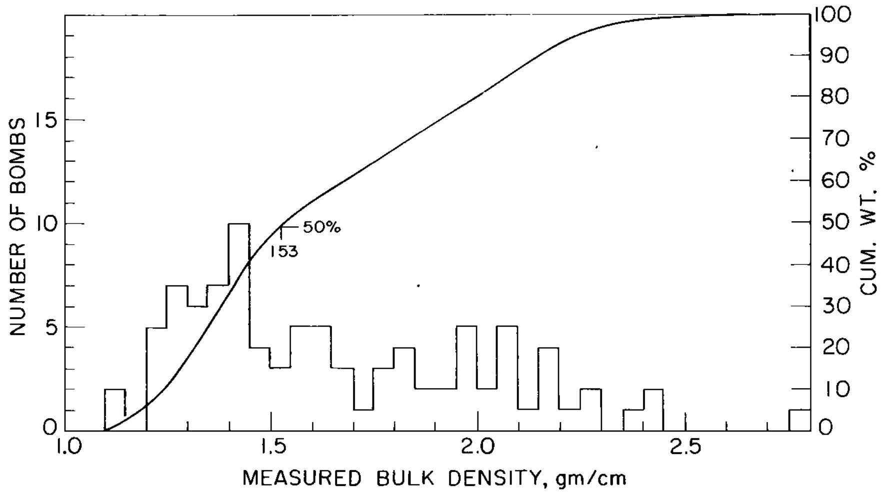

Fig. 10. Density of bombs from Northeast crater. A histogram and the distribution function for the density of 94 bombs from Northeast crater are shown. The median measured density was about 1.53 g/cm³.

angular distribution, radial symmetry being assumed. Ballistic calculations involving numerical integration of the particle trajectories were used to determine the exit conditions from the apex coordinates. The ballistic calculations used a drag coefficient that varies with Mach number (N. Hamisevicz and T. R. McGetchin, unpublished ballistic tables for earth, moon, and Mars, 1972).

The resulting distribution function describing the ejection velocity is shown in Figure 12. The median ejection velocity of particles in this particular eruption was about 51 m/s; the highest velocity was about 79 m/s, and the lowest was about 15 m/s. Fifty percent of the particles had exit velocities between 42 and 56 m/s; 90% had exit velocities between 34 and 62 m/s. For comparison, a similar curve is shown for Stromboli from data from high-speed movies taken during September 1971. Stromboli velocities (average about 25 m/s) are somewhat lower than the average Northeast crater values [*Chouet et al.*, 1974].

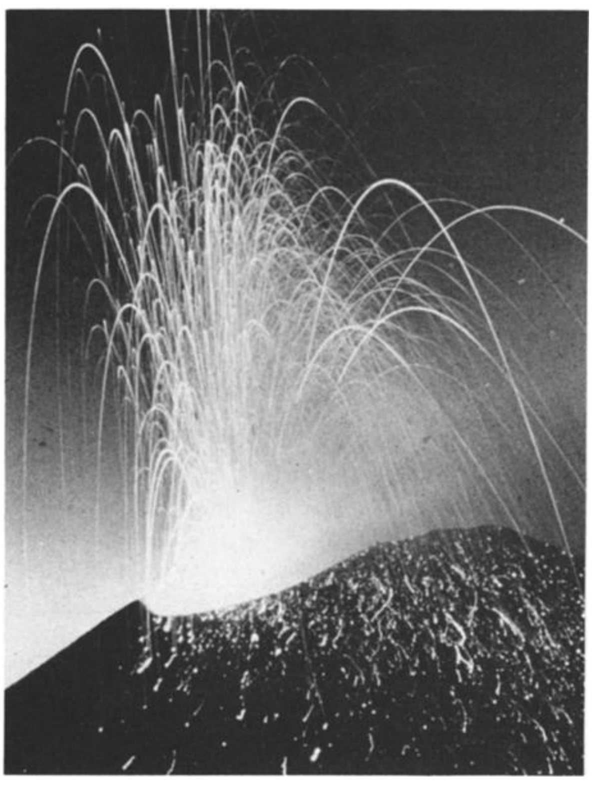

Fig. 11. Photograph of a typical eruption of Northeast crater during June 1969 taken from approximately the same location as Figure 6. This photograph was used in the ballistic analysis. Two hundred and eighty nine trajectories were located on the image, and their apparent exit angles and velocities were determined from the position of the apex of the trajectory, the effect of drag being included.

Most particles exit at very high angles, and the jet axis is apparently nearly vertical, as is revealed by observation from two sides of the cone. About 50% of the particles had apparent initial elevation angles (launch angle measured above the horizontal) of 85° or more; 90% were above 78°. When apparent elevation angles are converted to true elevation angles, the median angle is somewhat lower, about 79½°. The distribution of particles was slightly concentrated in the inside of the jet near 86° and somewhat depleted in the outer zones.

The ballistic range of a population of particles ejected at known exit conditions can be calculated directly by means of ballistics, including the effects of drag and gravity (Table 2). The distribution function describing the dispersion of ejecta with range was calculated for the particular exit conditions observed at Etna and for exterior ballistic conditions for the earth, Mars, and the moon. The elevation angles of ejected particles were assumed to be uniformly distributed in a cone

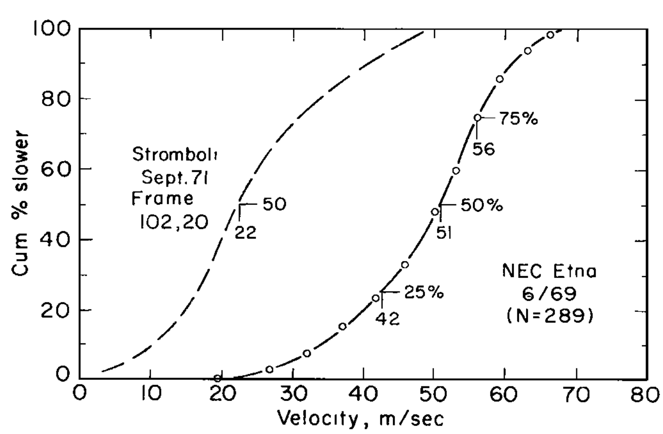

Fig. 12 Distribution function for exit velocities taken from Figure 11 For comparison, a similar curve for part of an eruption at Stromboli is shown from high-speed ballistic movie data.

TABLE 2. Ballistic Results for Launch Angles of 45°, 65° and 75°

V_0, m/s	Moon				Mars (ρ = 1.5 g/cm³, D = 10 cm)				Earth (ρ = 1.5 g/cm³, D = 10 cm)				Earth (ρ = 1.5 g/cm³, D = 100 cm)			
	R, m	t, s	Y_A, m	X/X_v	R, m	t, s	Y_A, m	X/X_v	R, m	t, s	Y_A, m	X/X_v	R, m	t, s	Y_A, m	X/X_v
45° launch angle																
10	61.8	8.7	15.5	1.00	26.7	3.78	6.7	1.00	9.9	1.43	2.5	0.967	10.2	1.45	2.5	1.00
30	557	26.2	139	1.00	237	11.3	59.9	0.986	31.2	4.1	19.9	0.775	89.2	4.4	22.5	0.972
100	6195	87.6	1549	1.00	2313	36.2	617.	0.865	235	9.4	111	0.280	774	13.3	218	0.759
300	56560	267	14140	1.00	10450	85.7	3510	0.433	502	14.1	255	0.055	2700	28.2	1005	0.294
65° launch angle																
10	47.4	11.2	25.4	1.00	20.5	4.85	11.0	1.00	7.5	1.83	4.1	0.965	7.8	1.85	4.2	1.00
30	426	33.6	228	1.00	182	14.5	97.9	0.985	53.7	5.1	31.9	0.763	68.2	5.5	37.0	0.969
100	4741	112	2541	1.00	1757	46.2	1001	0.858	204	11.6	166	0.261	584	16.9	350	0.747
300	42880	338	22990	1.00	7881	108	5438	0.427	341	17.8	362	0.049	1979	35.2	1534	0.281
75° launch angle																
10	30.9	12.0	29	1.00	13.4	5.2	12.4	1.00	4.2	1.85	4.7	0.966	5.9	1.97	4.7	1.00
30	278	35.8	260	1.00	119	15.4	111	0.986	35.3	5.4	36.2	0.769	44.6	5.9	42.0	0.970
100	3094	120	2885	1.00	1153	49	1134	0.862	134	12.3	185	0.263	334	18.0	396	0.753
300	27900	359	26020	1.00	5289	114	6109	0.439	222	18.3	398	0.048	1311	37.4	1718	0.285

Particle density of 1.5 g/cm³ from N. Hamisevicz and T. R. McGetchin (unpublished ballistics tables for the earth, moon, and Mars, 1972). V_0, initial velocity; R, range; t, flight time; Y, maximum height achieved; X/X_v, ratio of range attained by the particle (including atmospheric drag) to range attained by an identical particle in vacuum flight.

between 75° and the vertical, ejection velocities being distributed about a median of about 51 m/s and the maximum velocity being 70 m/s (Figure 12). To first order, we can assume that the elevation angle and the velocity are independent of each other.

About 5% of the particles fall within a range of 13 m on the earth, 56 m on Mars, and 132 m on the moon; 50% fall within 43, 203, and 494 m, respectively, and 90% fall within 71, 368, and 890 m, respectively. The ballistic limits of ejected particles (the maximum range attained by any ejected particle) for the three planets are 110 m for the earth, 750 m for Mars, and 1900 m for the moon.

The thickness of the ejecta can be calculated from the function $V(r)$, which describes the cumulative volumetric distribution of particles with range. The quantity $dV(r)/dr$ is the fraction of the total number of particles contained within a ring of width dr. The thickness $h(r)$ is the volume divided by the area over which this fraction is distributed, dA, and $dA = 2\pi r dr$. If the total volume is V_t, the thickness h is

$$h(r) = V_t \frac{dV(r)/dr}{dA(r)/dr} = \frac{V_t}{2\pi} \frac{dV(r)/dr}{r} \tag{1}$$

If the functional form of $V(r)$ is known, can be expressed analytically, and is differentiable, this equation can be solved and h expressed analytically. The distribution functions $V(r)$ for the earth, the moon, and Mars (Table 3) have no apparent simple analytic form, although several fits were attempted. Expressed as a power function of the form $V(r) = kr^a$, the value of the exponent was found to vary as a function of range nearly uniformly from 2.5 to zero. With $V(r)$ expressed in that way, the expression for thickness is

$$h = \frac{V_t \, d(kr^{a(r)})/dr}{2\pi r} \tag{2}$$

We note that the slope θ is given by dh/dr, so that taking the instantaneous derivative of (2) at $r = r$ (i.e., assuming $a(r) = a$ where a is approximately constant) yields

$$\theta = \frac{V_t k a}{2\pi} (a - 2) r^{a-3} \tag{3}$$

The slope by definition is zero at the rim (i.e., when $dh/dr = 0$ or when $a = 2$). The slope is also zero at $r = 0$, the center of the vent. From Table 3, $a = 2$ when the values of r are about 20, 88, and 206 m for the earth, Mars, and the moon, respectively, the location of the rim thereby being defined. We find that about 15% of the total volume of the ejecta lies within the rim, and 85% lies outside.

Since we found no simple analytical form for $V(r)$, the thickness as a function of range was evaluated by the numerical approximation

$$h(r) \sim V_t \frac{\Delta V}{2\pi r_m \cdot \Delta r} \tag{4}$$

where V_t is total crater volume and ΔV is the volume increment within an annular ring of width Δr centered at a radial distance r_m. For $V_t = 10^6$ m³ (approximately the volume of Northeast crater) the resulting rim heights H are 125, 5.6, and 0.98 m for the earth, Mars, and the moon, respectively. (The 125-m height for the earth is unreasonable since it ignores the collapse of slopes, which, by this model, would have been built too well beyond the angle of repose. As will be shown

TABLE 3. Distribution of Particles With Function Range Resulting From Ejection at Certain Conditions

		Range, m		
$V(r)$*	$a(r)$†	Earth	Mars	Moon
5	2.3	13	56	132
10	2.1	16	72	171
15	2.0	20	88	206
25	1.8	28	119	280
50	1.4	43	203	494
75	1.0	57	301	713
90	0.7	71	368	890
95	0.5	75	404	1004
99	0.2	82	468	1169
100	0.0	110	750	1900

Ejection angles are distributed uniformly between 75° and 90°; velocities are distributed as observed at Northeast crater; exterior ballistic environment is appropriate for indicated planet.
*Cumulative volume.
†Slope of cumulative volume curve.

shortly, collapse of these oversteepened slopes to about 30° produces a cone of height near 59 m.) The location or range of the rim R does not change with total volume, whereas the rim height H varies directly with volume (until slopes grow to the point where the walls fail by slumping).

We now use these results to discuss two problems, the changing shape of cinder cones during their growth and the predicted cone profiles for cinder cones on the moon and Mars.

Growth of Northeast Crater

The present volume of Northeast crater is about 1×10^6 m^3. If the identifiable particles ejected (in the eruption of June 1969) are assumed to average about 10 cm in diameter (0.0005 m^3) and if about 300 particles are ejected per eruption, the approximate volume ejected is 0.15 m^3 per eruption. If the irregular shape of the particles, the inefficient packing, and the small particles below the resolution limit of the photograph are taken into account, one such eruption might contribute 0.15–0.5 m^3 per nominal eruption. Therefore between 2 and 7 $\times 10^6$ eruptions were required to produce the present volume of Northeast crater in its 60-year history since 1911 (3.2×10^7 min). The implied eruption frequency of one every 4.5–16 min is in reasonable agreement with the observed rate.

If Northeast crater was built by n repeated eruptions (about 2–7 million over 60 years) similar to the eruption analyzed, the crater profile evolves as predicted by the previous equations for $h(r, V_t)$. Cinder cone growth according to this model is shown in Figure 13. The model predicts that at a volume of 0.25×10^6 m the rim would be about 30 m high, a very steep slope beginning to develop at a range of about 20–25 m. At 0.5×10^6 m^3 the calculated rim is about 62 m high, the slope at about a 25-m range continues to steepen to about 60° at this volume, well beyond anything reasonably stable, and the ejecta layer is less than 1 m deep at a 100-m range. At a cone volume equal to about 1×10^6 m^3 the slope of the outer surface will be determined entirely by collapse of the oversteepened slope rather than by ballistics. If we assume that the rim location remains approximately at a 16-m range, the resulting cone, produced by collapse of ejecta into talus at 30° (outward and inward dip from the rim), would have a height of about 59 m, a radius of just over 118 m, and an internal conical crater 10 m deep. For the ballistic conditions of ejecta distribution inferred for Northeast crater the first talus slope will form at a range of about 20–25 m when the cone volume is approximately 0.2×10^6 m^3 (Figure 13). Addition of more volume results in an oversteepening of the slope, and a portion of the upper part of the slope will slump downward. As the cone volume increases, a large talus pile will evolve. For this particular model at about 0.2×10^6 m^3 the cinder cone evolves from a simple structure with a low rounded rim and similar internal bedding to one with an external outward-dipping talus slope.

The agreement between predictions and observations is quite good at Northeast crater. The actual profile of the crater fits the calculated models very well for the true volume of Northeast crater of about 1×10^6 m^3. This fit probably means that the eruption conditions derived from photographic analysis are nearly typical of those that produced Northeast crater, but the model does ignore the few but important large eruptions. Also, many cinder cones are composite; that is, they consist of interbedded flows and pyroclastics. The interbedded flows will freeze the development of a surface and may introduce their own geometric complications, such as reducing the exterior slope of the cone.

The morphological properties and the sequence of events in the formation of an idealized cinder cone implied by the preceding development are shown in Figure 14. The location of the rim and the ballistic limit are uniquely defined by the exit conditions (the joint distribution function describing velocity and exit angle) and the exterior ballistic environment. The limit of continuous ejecta (defined as the range where ejecta thickness equals the average particle size), the rim height, and the characteristics of the talus pile (its volume and the location of the top and bottom) are uniquely determined by the exit conditions, the total cone volume, and gravity and

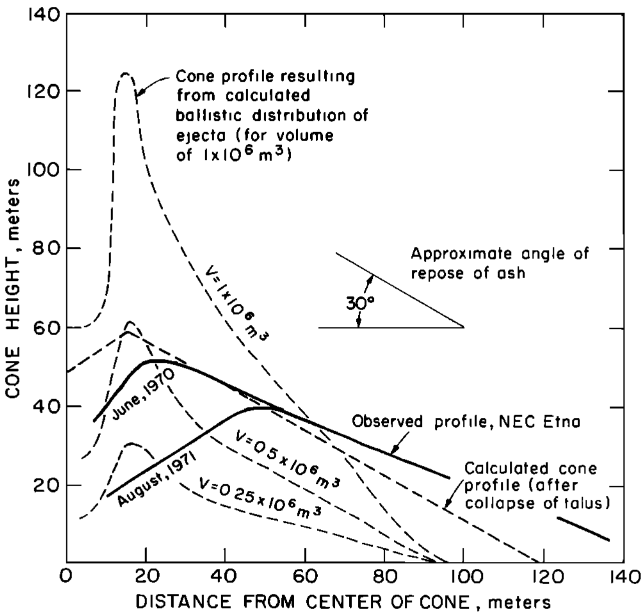

Fig. 13. Growth of Northeast crater as a function of crater volume. Cone profiles were calculated by using the ballistic distribution of particles resulting from the specific exit conditions observed in the eruption photograph, varying only total cone volume. In this model at a volume of about 0.2×10^6 m^3 the outer slope of the crater reaches 30°, the approximate angle of repose. Addition of more ejecta oversteepens the slope, and the volume slumps, a talus slope thus being produced. The approximate true profiles of Northeast crater are shown. The rim is located at 59 m for the model, regardless of total volume.

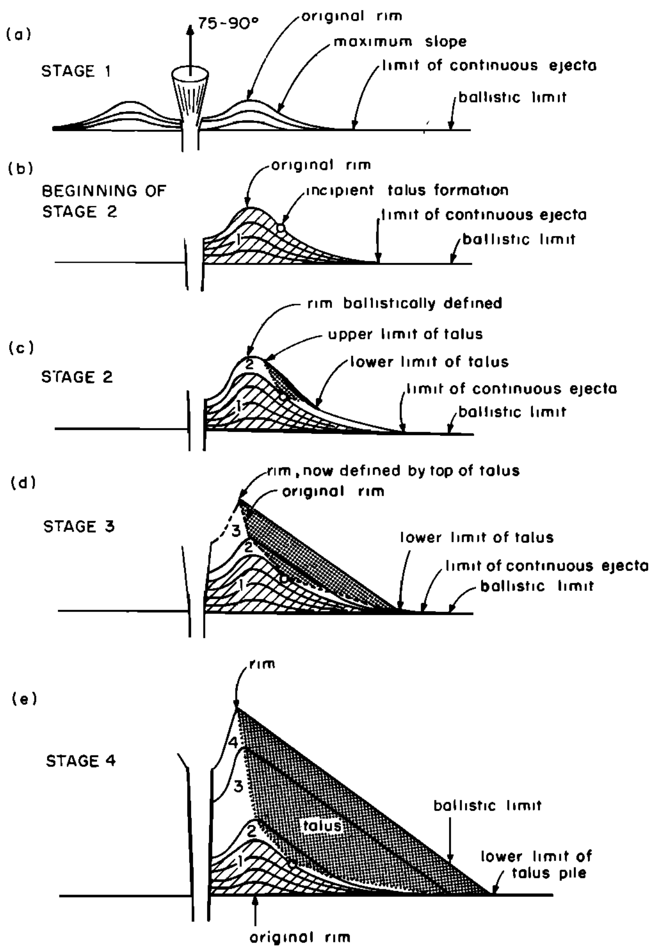

Fig. 14. Four major stages of the development of cinder cones. Stage 1 (*a*) is a low-rimmed mantle-bedded pyroclastic ring. Stage 2 (*b* and *c*) begins with the development of exterior talus. Stage 3 begins with the destruction of the original rim by inward migration of the talus pile (*d*). In stage 4 (*e*) the volume of the cone grows, so that talus extends beyond the ballistic limit of ejecta. Martian and lunar cinder cones probably rarely evolve past stage 1 unless they have far greater volume than their terrestrial counterparts.

atmospheric conditions. More specifically, cinder cones develop through the following four idealized stages.

In eruptions producing cinder cones, ejecta exits at velocities distributed about some mean and at high angle, to first order, in a cone between about 75° and 90° from the horizontal. This material distributes itself according to the detailed statistical nature of the relationship between exit angle and exit velocity and the effects of atmospheric drag and cross wind.

If the eruptions are identical, or approximately so, and the atmosphere is calm, a simple symmetrical cone with a low rounded rim forms (a simple cone of stage 1). Bedding will be precisely similar. The location of the rim does not migrate as the crater grows, the limit of continuous ejecta moves outward, and the ballistic limit is fixed. The location (range) of the maximum outward-dipping slope does not change; its location is given by maximizing dh/dr. Notice that $dh/dr = 0$ at the rim and at the vent.

As the cone grows by addition of n similar beds, the dimensionless crater profile does not change (h/H, r/R). At some ejecta volume, depending on the exit conditions, the slope of the outer surface of the crater equals the angle of repose of the material on the slope (about 31°–38°, depending on the material). At that volume incipient talus forms. Addition of further material results in oversteepening of the slope and talus development, and thus the transition from stage 1, a simple cone, to stage 2, a cone with an outward-dipping talus slope, is marked.

A cone having a volume in excess of the limit for a simple cone will develop a talus ring extending from somewhere below its well-rounded rim to a nick point at the base of the cone. As volume increases, the talus pile migrates upward toward the original rounded rim and outward along the base, more and more ballistically emplaced ejecta being progressively overlapped. Stage 2 cones still have a round rim whose location is determined by the ballistic conditions of ejecta.

As the crater continues to grow, the inward migration of the upper part of the talus pile eats through the original rounded rim. At volumes exceeding the stage 2 volume, the rim is located at ranges less than the original ballistically determined rounded rim. Also, by this stage severe modification of the interior of the cone may occur through collapse of the vent, talus formation on the inner slopes, or destruction by large eruptions resulting from clogging of the vent. The destruction of the old rounded rim by the inward migration of the upper edge of the talus pile marks the transition between stages 2 and 3. Stage 3 cones have no rounded rim and a very well developed and wide outer talus pile.

Further addition of ejecta extends the limits of the talus pile until eventually its outer edge overrides the ballistic limit of the trajectories of ejected particles, and a stage 4 cone is produced. Beyond this volume the cone grows as a simple conical pile of cinders at the angle of repose.

The internal structure of large conical cinder cones (and probably many stratovolcanoes) can be inferred from this development. The base is a simple stage 1 cone with a well-rounded rim and simple similar bedded layers. On top of the simple stage 1 cone is a stage 2 cone with its incipient to well-developed talus slope. One might infer that as the talus pile grows, a ring of coarse fragments marks its base; the fragments become larger as the talus pile grows because the sorting mechanism (by boulder rolling) becomes more efficient. As the cone grows, the extent of the talus pile grows through stages 3 and 4. The inferred internal structure of Etna's Northeast crater shown in Figure 7 corresponds to a late stage 3 or early stage 4 cone.

These results suggest that the formation conditions can be inferred from the cone shape if certain reasonable assumptions are made about the distribution of particles in the exit jet. In other words, the detailed crater shape can be inverted to determine the distribution function for velocity if a reasonable estimate can be made of the distribution function for exit angle. This is of considerable interest for both terrestrial and planetary surface applications because volcanic exit conditions are related to such generally interesting properties as temperature and the volatile content of the erupting system as well as to the exterior ballistic environment, including wind.

The inferred stages of growth of Northeast crater are in good agreement with the observed growth of Parícutin during 1943 and 1944. In particular, the external cone profiles drawn by *Foshog and Gonzalez* [1956, p. 448, Figure 122] are in excellent agreement with our Figure 14. The location of the rim of Parícutin on February 23, 1943, just after its formation was at a range of about 60 m, considerably greater than that at Northeast crater. The external talus slope was developed at that time, and the cone height was about 50 m. As the cone grew, the rim location migrated outward to greater ranges and was defined by the intersection of outward- and inward-dipping talus deposits. During the early eruptions, bombs were lofted to a height of 500 m and landed at ranges of about 400 m. When a bomb density of 1.5 g/cm^3 and a diameter of 10 cm are assumed, they imply an exit velocity of about 600 m/s, an elevation angle of approximately 65° (N. Hamisevicz and T. R. McGetchin, unpublished ballistic tables, 1972), a considerably higher velocity, and somewhat lower launch angles than those observed at Northeast crater.

Scott and Trask [1971] reported 17 carefully surveyed Quaternary cinder cones in Nye county, Nevada, and published detailed cone profiles. Heights vary from 60 to 200 m, base radii vary from 250 to about 980 m, slopes vary from 21° to 33°, and rim radii vary from about 130 to 300 m. They also define a parameter *S*, the length of constant exterior slope, which we would interpret to be talus as described in Figures 13 and 14. The ratio *S*/*h* (where *h* is cone height) is 0.7–1.4. Northeast crater at Mount Etna is similar to the small geomorphically fresh cones described by Scott and Trask, but it has an *S*/*h* of about 2.3 and a smaller rim radius. The Nye county, Nevada, cones appear to be stage 3 cinder cones as defined in Figure 15.

MARTIAN AND LUNAR CINDER CONES

If Northeast crater erupted on Mars or the moon, the ejecta would be ballistically distributed according to the exit angles, velocities, and gravity and atmospheric conditions, including deceleration of particles by drag and cross wind effects. The initial ejection conditions (especially velocity) are probably somewhat gravity dependent [*McGetchin and Ullrich,* 1973], and the exit angles may be influenced by the pressure and density of the ambient atmosphere. Trajectories of 1- to 10-cm particles exiting at typical cinder cone conditions (~50 m/s and 70°–80°) attain about 25–50% of their vacuum range; on Mars the same particles would attain 75–95% of their vacuum range (Figure 15). An eruption into the vacuum at the moon's surface will result in vigorous upward and sidewise expansion of some of the entraining gas in the jet, especially near the boundary [*Greenspan and Butler,* 1962]. This expansion will tend to give a horizontal component of velocity to the particles entrained in the outer edges of the jet. The trajectories of some particles will be perturbed, depending on their size, density, and shape and their position relative to the axis of the jet. The exit velocity attained by most entrained particles may not be significantly affected. Some of these factors are subject to experiment or analysis, whereas others will require geological observations on the moon and Mars. McGetchin and Ullrich's calculated results for the exit velocity of fragments ejected from diatremes suggest that particles of equivalent size are ejected at about 80 and 60% of their terrestrial velocity on Mars and the moon, respectively, all eruption parameters being equal. The ballistic range of particles as a function of exit velocity (including atmospheric drag with the appropriate atmospheres for the earth, Mars, and the moon) is shown in Figure 16.

Let us assume that lunar and Martian cinder cones erupt with about the same exit conditions as terrestrial ones (in particular, with the exit conditions observed at Northeast crater). We can inquire about the crater shapes resulting from repeated eruptions similar to those of Northeast crater if they occurred on Mars and the moon. The crater profiles resulting from 1 × 10^6 m^3 of material ejected at Northeast crater conditions produce cinder cones with exceedingly different shapes on the earth, Mars, and the moon (Figure 17). The properties of these cones are summarized in Table 4.

On the earth, such a cone has a rim about 59 m high located about 16 m from the center of the cone and a well-developed outward-dipping talus slope extending all the way from the rim to the base of the cone at 118 m. The ballistic limit is at about 110 m, and the limit of continuous ejecta is at 118 m as defined by slope collapse and talus development rather than by ballistic considerations. Typical flight times of ejecta are

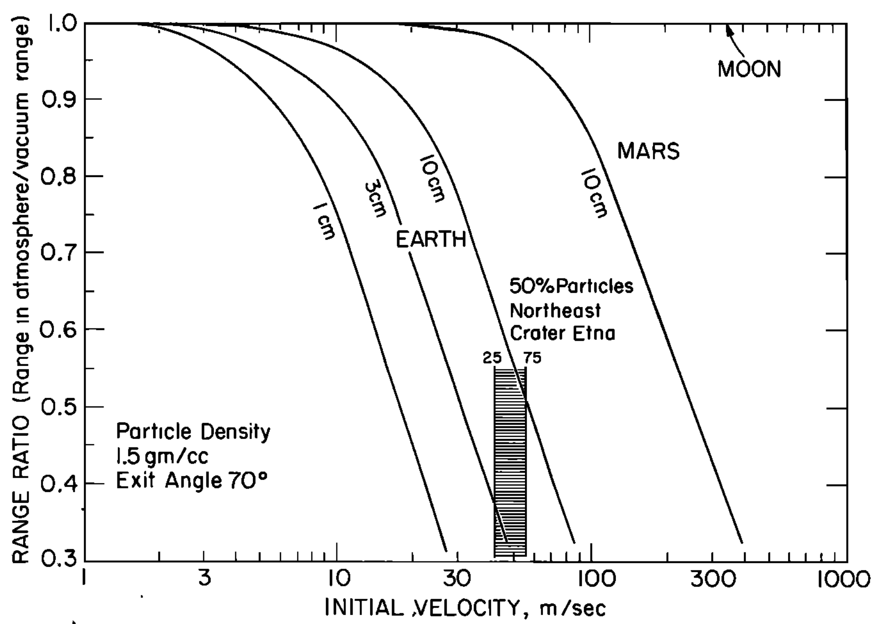

Fig. 15. Fraction of vacuum ballistic range attained by ejecta particles on the earth, the moon, and Mars as functions of initial velocity and particle size for a particle density of 1.5 g/cm^3 and a launch angle of 70° above the horizontal. The shaded zone shows the exit velocity of 50% of the Northeast crater ejecta. On the earth such ejecta attains only about 50% of its vacuum range; on Mars it attains over 95%, and on the moon it attains 100%.

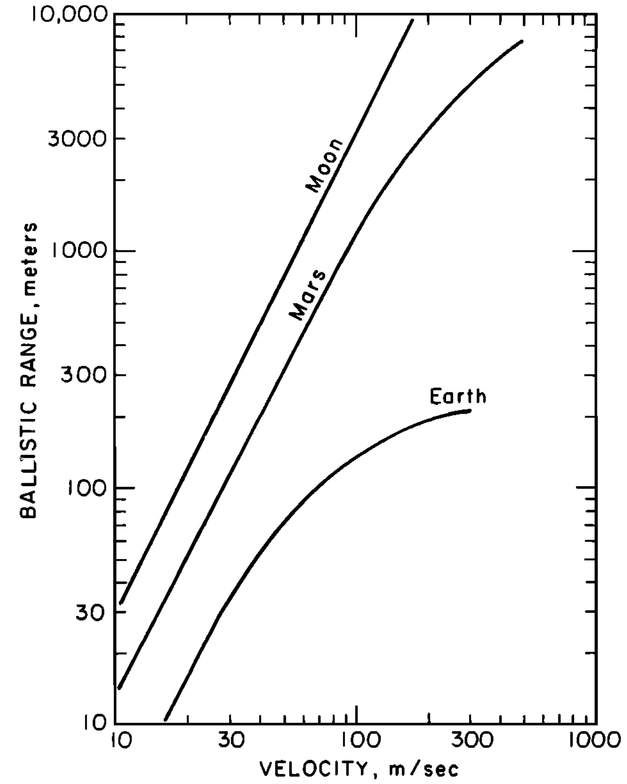

Fig. 16. Particle range as a function of exit velocity for ballistic trajectories in the appropriate atmosphere for the earth, Mars, and the moon. The calculations include the effect of atmospheric drag and assume a still atmosphere (no cross wind), a particle diameter of 10 cm, a density of 1.5 g/cm³, and a launch angle of 75° above the horizontal.

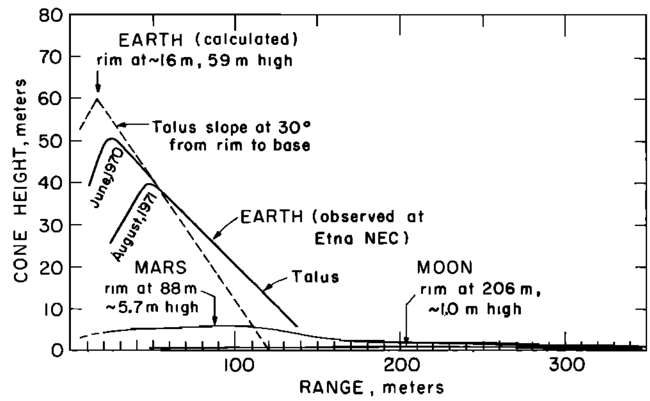

Fig. 17. Comparison of profiles for cinder cones of volume 1 × 10⁶ m³ erupted at conditions observed at Northeast crater onto the surface of the earth, Mars, and the moon. Vertical exaggeration 2.5×.

5–10 s; hence the center of large fragments will hit the ground in a molten state.

On Mars the same volume (1 × 10^6 m^3) would be distributed so that the rim is about 6 m high and is located at an 88-m range. No talus is developed on the outer slope of the crater because slopes are small; the limit of continuous ejecta will be at about 420 meters, and the ballistic limit of ejecta is about 750 m. Typical flight times are 15–30 s.

On the moon a broad flat cone with a barely discernible rim about 1 m high is produced at a range of 210 m; the limit of the continuous ejecta occurs at about 1025 m, and the ballistic limit of ejecta is at about 1900 m. Typical flight times of ejecta are of the order of 1 min, sufficient for most particles to be quite cool upon hitting the ground.

Hence in lunar conditions an ordinary terrestrial cinder cone would have the appearance of a maar or an ash ring. The smaller dark halo craters that have received attention as possible sources of deep-seated xenoliths may be only the natural lunar form of common cinder cones. If lunar cinder cones occur as clusters in cone fields, as they do on the earth (commonly numbering several hundred cones spaced 2–5 km apart), they would produce blankets similar to the young dark mantle units circumferential to some lunar mares. If most of the source vents are closely spaced, the first vent to erupt may be buried by ejecta from subsequent eruptions, only the latest vents being visible.

TABLE 4. Summary of Properties of Craters Produced by Ejection of 1 x 10^6 m^3 of Material at Conditions of the June 1969 Eruption at Northeast Crater, Mount Etna

	Earth	Mars	Moon
Rim height, m	125 (59 after slumping)	6	1
Rim location, range, m	∿16	88	206
Maximum slope, deg	30 from rim to 118 m	About 10 at 150 m	About 0.4 at 350 m
Talus development	Well developed	None	None
Limit of continuous ejecta, m	∿118	∿420	∿1025
Limit of ejecta (ballistic limit), m	∿110	∿750	∿1900
Typical flight time of ejecta, s	5 to 10	15 to 30	40 to 80
Appearance in 3.8-cm radar	Bright ring at base of talus slope; cinder cone bright.	Bright inside rim; outside ejecta probably dark.	
Appearance in 70-cm radar	Bright locally at base of talus slope ringing crater; otherwise dark.	Dark everywhere	
IR anomaly	Strong at crater.	Probably none.	

Cross-polarized radar reflections from planetary surfaces yield data regarding particle size relative to the wavelength of the radar (3.8 and 70 cm). Typically, volcanic ash has a median grain size on the 100-μ scale. The bulk ejecta from Northeast crater (believed to have an average size of about 1 cm) would have a dark reflection in both the 3.8- and the 70-cm radar because most of the surface would consist of particles smaller than the wavelength of the radar. The ring of coarse fragments collected at the base of the talus pile at Northeast crater would produce a locally strong radar reflection in the form of a narrow annular ring. Large fragments concentrated near and on the rim (owing to their lower exit velocities) would produce a bright reflection near and inside the rim. The windward side of Northeast crater is covered with 10-cm bombs and hence would appear dark in 70-cm radar and bright in 3.8-cm radar. If the Martian surface is continuously subjected to strong wind, fine ash will be winnowed away and coarse fragments enhanced, and the cones produced may be asymmetrical simple cones (stage 1 type). The asymmetry will reflect the wind environment [*Greeley et al.*, 1974]. Lunar cinder cones probably are symmetrical, and we would expect a dark reflected radar backscatter. If volatiles are trapped in the glass, the dielectric constant will be higher and the radar reflection weaker (i.e., even darker) owing to absorption of some of the signal (S. Zisk, personal communication, 1972).

Pyroclastic volcanic ejecta is not widely dispersed on the moon from its source by the original eruptive event if it is ejected at conditions approximately like those of Northeast crater (Figure 16). In this case the observed mixing of pyroclastic fragments to great distances and admixture into the lunar regolith are dependent on impact mechanisms and age. The Apollo 11, 12, 14, 15, and 16 landing sites are not close to any known dark halo craters. Part of the dark blanketing deposits near Littrow (Apollo 17), however, may be lunar counterparts of terrestrial cinder cones [*McGetchin and Head*, 1973] or lava fountains [*Heiken et al.*, 1974].

Flight times for material ejected on the moon are substantially longer than those for the earth or Mars. Flight times of about 1 min should be normal on the moon, sufficient for radiative cooling of most particles to subsolidus temperatures; hence little or no welding of cinder cone ejecta should be expected on the moon.

Finally, one important general conclusion of this study is that genetic arguments based on morphological similarities of observed planetary and terrestrial surface features should be treated with much caution and accepted only to the extent that sufficient understanding of physical mechanisms permits construction of realistic models for their formation. Our results clearly show that features with similar origins may have very different appearances in other planetary environments. Lookalike features may have quite different origins, and one may unwittingly be comparing features that fortuitously look alike because of environmental differences.

On the positive side, fundamental understanding of formation processes may permit interesting inferences to be drawn about planetary environments from analysis of landforms. For example, in the case of cinder cones we feel that topographic shape, ultimately, can be inverted with reasonable confidence to infer both the exit conditions and some details of the exterior ballistic environment, particularly cross winds. Both are of considerable interest because the exit conditions, particularly particle velocities, are related to the volatile content of the erupting medium. Wind direction and magnitude are clearly of interest on Mars.

Acknowledgments. We are grateful to Richard Birnie of Harvard and to Douglas Hopkins of MIT for assistance in the field; to Antonio Nicoloso of Sapienze for generosity and many courtesies extended to us while we were in Sicily; to H. Tazieff and F. LeGuern and their field team for graciously sharing their facilities and offering good company in the field; to R. Romano and A. Rittman for assistance with logistical problems in Catania; and to Sue Hall and Penny Sharp for help with the preparation and logistics of the field trip and preparation of the manuscript. This research was supported by grants from the planetology office, NASA (NGR 22-009-637 and NSG 07012). We are most grateful for the support. Helpful reviews of the manuscript were provided by Dallas Peck, Robert P. Sharp, Grant Heiken, and Charles Wood.

References

Becker, G. F., The geometric form of volcanic cones and the elastic limit of lava, *Amer. J. Sci.*, *30*, 283–293, 1885.

Bullard, F. M., *Volcanoes, in History, in Theory, in Eruption*, pp. 70–91, University of Texas Press, Austin, 1962.

de Bruyn, J. W., Isogam maps of Europe and North Africa, *Geophys. Prospect.*, *3*, 1–14, 1955.

Chouet, B. A., Photoballistic analysis of volcanic jet dynamics at Stromboli, Italy, M. S. thesis, Mass. Inst. of Technol., Cambridge, 1973.

Chouet, B. A., N. T. Hamisevicz, and T. R. McGetchin, Photoballistics of volcanic jet activity at Stromboli, Italy, submitted to *J. Geophys. Res.*, 1974.

Cotton, C. A., *Volcanoes as Landscape Forms*, 416 pp., Whitcombe and Tombs, Christchurch, New Zealand, 1944.

Eaton, G. P., Windborne volcanic ash—A possible index of polar wandering, *J. Geol.*, *72*, 1–35, 1964.

Erikson, A. J., The measurement and interpretation of heat flow in the Mediterranean and Black Sea, Ph.D. thesis, Mass. Inst. of Technol., Cambridge, 1970.

Fahlquist, D. A., Seismic refraction measurements in the western Mediterranean Sea, Ph.D. thesis, Mass. Inst. of Technol., Cambridge, 1963.

Fisher, R. V., Maximum size, median diameter, and sorting of tephra, *J. Geophys. Res.*, *69*, 341–355, 1964.

Fisher, R. V., and A. C. Waters, Base surge bed forms in maar volcanoes, *Amer. J. Sci.*, *268*, 157–180, 1970.

Foshog, W. F., and J. Gonzalez, Birth and development of Parícutin volcano, Mexico, *U.S. Geol. Surv. Bull.*, *965-D*, 355–489, 1956.

Gasparini, P., and J. A. S. Adams, K-Ar dating of Italian Plio-Pleistocene volcanic rocks, *Earth Planet. Sci. Lett.*, *6*, 225–230, 1969.

Girdler, R. W., Drifting and rifting of Africa, *Nature*, *217*, 1102–1106, 1968.

Greeley, R., J. D. Iversen, J. B. Pollack, N. Udovich, and B. White, Wind tunnel simulations of light and dark streaks on Mars, *Science*, *183*, 847–849, 1974.

Green, J., and N. M. Short, *Volcanic Landforms and Surface Features*, pp. 48–58, Springer, New York, 1971.

Greenspan, H. P., and D. S. Butler, On the expansion of a gas into vacuum, *J. Fluid. Mech.*, *13*, 101–119, 1962.

Heiken, G. H., Tuff rings: Examples from the Fort Rock–Christmas Lake valley basin, south-central Oregon, *J. Geophys. Res.*, *76*, 5615–5626, 1971.

Heiken, G. H., Morphology and petrology of volcanic ashes, *Geol. Soc. Amer. Bull.*, *83*, 1961–1988, 1972.

Heiken, G. H., D. S. McKay, and R. W. Brown, Lunar deposits of possible pyroclastic origin, *Geochim. Cosmochim. Acta*, in press, 1974.

Imbo, G., *Catalog of Active Volcanoes of the World*, part 18, *Italy*, p. 40, International Association of Vulcanology, Rome, 1965.

Jagger, T. A., Origin and development of craters, *Geol. Soc. Amer. Mem.*, *21*, 1–508, 1947.

Kieffer, G., Une ultime phase d'activité explosive de la Valle del Bove (Etna) vieille de 5000 ± 130 ans et ses enseignements sur l'histoire recente du grand volcan sicilien, *C. R. H. Acad. Sci*, *270*, 3198–3201, 1970.

Klerkx, J., La présence d'une clastolave dans la Valle del Bove (Etna), *Geol. Rundsch.*, *57*, 737–744, 1968.

Klerkx, J., Le caldera de la Valle del Bove: Sa signification dans l'évolution de l'Etna (Sicile), *Bull. Volcanol.*, *34*, 726–737, 1971.

Knox, J. B., and N. M. Short, A diagnostic model using ash fall data to determine eruption characteristics and atmospheric conditions during a major volcanic event, *Bull. Volcanol.*, *27*, 5–24, 1964.

Lamb, H. H., Volcanic dust in the atmosphere; with a chronology and assessment of its meteorological significance, *Phil. Trans. Roy. Soc., London, Ser. A, 266,* 428–533, 1970.

Lyell, C., On craters of denudation, with observations on the structure and growth of volcanic cones, *Quart. J. Geol. Soc. London, 6,* 207–234, 1850.

Macdonald, G. A., *Volcanoes,* pp. 183–195, Prentice-Hall, Englewood Cliffs, N. J., 1972.

McGetchin, T. R., and J. W. Head, Lunar cinder cones, *Science, 180,* 68–71, 1973.

McGetchin, T. R., and G. W. Ullrich, Xenoliths in maars and diatremes, with inferences for the moon, Mars, and Venus, *J. Geophys. Res., 78,* 1833–1853, 1973.

McKenzie, D. P., Plate tectonics of the Mediterranean region, *Nature, 220,* 239–243, 1970.

Moore, J. G., R. Cristogoline, and A. LoGiudice, Development of pillows on the submarine extension of recent lava flows, Mount Etna, Sicily, *U.S. Geol. Surv. Prof. Pap., 750-C,* 89–97, 1971.

Pichler, H., Volcanism in eastern Sicily and the Aeolian Islands, in *Geology and History of Sicily,* edited by W. Alvarez and K. H. A. Gohrbandt, pp. 261–281, Petroleum Exploration Society of Libya, Tripoli, 1970.

Porter, S. C., Distribution, morphology and size frequency of cinder cones on Mauna Kea volcano, Hawaii, *Geol. Soc. Amer. Bull., 83,* 3607–3612, 1972.

Rittmann, A., Vulkanismus und Tektonik des Aetna, *Geol. Rundsch., 53,* 788–800, 1963.

Rittmann, A., Notizie sull' Etna, 4, *Suppl. Nuovo Cimento, Ser. 1, 3,* 1117–1123, 1965.

Rittmann, A., The Mt. Etna eruption of 1971, in *Annual Report,* p. 68, Smithsonian Center for Short-Lived Phenomena, Cambridge, Mass., 1971.

Romano, R., Tectonic control on magmatic differentiation: An example, *Bull. Volcanol., 34,* 823–832, 1970.

Ryan, W. B. F., D. J. Stanley, J. B. Hersey, D. A. Fahlquist, and T. Allan, The tectonics and geology of the Mediterranean Sea, in *The Sea,* vol. 4, edited by A. E. Maxwell, pp. 387–492, John Wiley, New York, 1971.

Scott, D. H., and N. J. Trask, Geology of the lunar crater volcanic field, Nye county, Nevada, *U.S. Geol. Surv. Prof. Pap., 599-I,* 1–22, 1971.

Sheridan, M. F., Particle size characteristics of pyroclastic tuffs, *J. Geophys. Res., 76,* 5627–5634, 1971.

Stanley, D. J., and E. Mutti, Sedimentological evidence for an emerged land mass in the Ligurian Sea during the Palaeogene, *Nature, 218,* 32–36, 1968.

Stearns, H. T., and G. A. MacDonald, Hawaiian lava production rates, *Hawaii Div. Hydrogr. Bull., 9,* 1–363, 1946.

Swanson, D. A., Magma supply rate at Kilauea volcano, *Science, 175,* 169–170, 1971.

Tanguy, J. C., Les laves récentes de l'Etna, *Bull. Soc. Geol. Fr., 8,* 201–217, 1966.

Tanguy, J. C., Présence de basaltes à caractere tholeiitique dans la zone de l'Etna (Sicile), *C. R. H. Acad. Sci., 264,* 21–24, 1967.

Tanguy, J. C., Relation entre structures petrographiques de quelques laves de l'Etna et les conditions volcanologiques de leur mise en place, *Bull. Volcanol., 32,* 177–187, 1968.

Tanguy, J. C., Mt. Etna volcanic eruption, in *Annual Report,* pp. 61–69, Smithsonian Center for Short-Lived Phenomena, Cambridge, Mass., 1971.

Tazieff, H., Mount Etna: Its present volcanic activity and associated volcanological research, in *Geology and History of Sicily,* edited by W. Alvarez and K. H. A. Gohrbandt, pp. 285–291, Petroleum Exploration Society of Libya, Tripoli, 1960.

Tazieff, H., *Field Excursion Guide to Mt. Etna,* Instituto Internazionale di Vulcanologia, Catania, Italy, 1971.

Thorarinsson, S., Laxargljufur and Laxarhraun, a tephrachronological study, *Mus. Natur. Hist. Reykjavik Misc. Pap., 2,* 1–88, 1951.

Thorarinsson, S., The eruption of Hekla, 1947–1948, 1, The eruptions of Hekla in historical times, a tephrachronological study, *Soc. Sci. Island. Reykjavik, 1,* 1–170, 1967.

Walker, G. P. L., Thickness and viscosity of Etnean lavas, *Nature, 213,* 484–485, 1967.

Waters, A. C., and R. V. Fisher, Base surges and their deposits, Capelinhos and Taal volcanoes, *J. Geophys. Res., 76,* 5596–5614, 1971.

Wilcox, R. E., Some effects of recent volcanic ash falls with especial reference to Alaska, *U.S. Geol. Surv. Bull., 1928-N,* 409–476, 1959.

(Received November 17, 1972;
revised May 2, 1974.)